Morphology of the Small-Animal Lung Using Magnetic Resonance Microscopy

Laurence W. Hedlund and G. Allan Johnson

Center for In Vivo Microscopy, Duke University Medical Center, Durham, North Carolina

Small-animal imaging with magnetic resonance microscopy (MRM) has become an important tool in biomedical research. When MRM is used to image perfusion-fixed and "stained" whole mouse specimens, cardiopulmonary morphology can be visualized, nondestructively, in exquisite detail in all three dimensions. This capability can be a valuable tool for morphologic phenotyping of different mouse strains commonly used in genomics research. When these imaging techniques are combined with specialized methods for biological motion control and animal support, the lungs of the live, small animal can be imaged. Although *in vivo* imaging may not achieve the high resolution possible with a fixed specimen, dynamic functional studies and survival studies that follow the progression of pulmonary change related to disease or environmental exposure are possible. By combining conventional proton imaging with gas imaging, using hyperpolarized ^{3}He, it is possible to image the tissue and gas compartments of the lung. This capability is illustrated in studies on an emphysema model in rats and on radiation damage of the lung. With further improvements in imaging and animal handling technology, we will be able to image faster and at higher resolutions, making MRM an even more valuable research tool.

Keywords: fixed specimens; *in vivo*; lung; magnetic resonance microscopy; rodent

Small-animal imaging has assumed an important role in biomedical research involving rodent models of human disease (1, 2), drug development (3), toxicology (4), and morphologic phenotyping in the genomics community (5, 6). This role is partly due to its ability to image the whole animal body and visualize the three-dimensional (3D) morphology nondestructively. Also important is its ability to noninvasively examine changes in specific organs on a regional, 3D basis. This is particularly true for small-animal models of pulmonary disease, such as asthma, emphysema, edema, and fibrosis (7–9). Imaging the lungs is an especially challenging task due to low density and constant motion, and, with magnetic resonance (MR), the task is even more difficult because of the air–tissue interface susceptibility effects that further reduce signal strength (10).

This article covers the challenges and solutions for using MR to image the small-animal lung in the microscopic domain from the standpoints of the physics and biology. We show examples of MR imaging (MRI) of the lungs with the highest resolution possible using perfusion-fixed specimens and consider the special issues of high-resolution lung imaging in the live, small animal.

(*Received in original form July 29, 2005; accepted in final form August 24, 2005*)

Supported by National Institutes of Health grants NCRR P41 RR005959, NCI R24 CA092656, and NHLBI R01 HL055348.

Correspondence and requests for reprints should be addressed to Laurence W. Hedlund, Ph.D., Center for In Vivo Microscopy, Box 3302, Duke University Medical Center, Durham, NC 27710. E-mail: laurence.hedlund@duke.edu

The color figures for this article are on pp. 501–502.

Proc Am Thorac Soc Vol 2. pp 481–483, 2005
DOI: 10.1513/pats.200507-074DS
Internet address: www.atsjournals.org

CHALLENGES FOR MR MICROSCOPY OF THE LUNG OF SMALL ANIMALS

MR microscopy (MRM) is a logical extension of the principles and technology used in clinical MRI—from the whole body scanner for humans (70 kg) to specialized systems for rats (0.250 kg) and mice (0.030 kg). A major challenge for the development of MRM has been contending with the greatly reduced signal intensity associated with the microscopic voxel volumes. Voxels less than 0.03 mm^3 in volume are generally labeled "microscopic" to indicate spatial resolution finer than that discernible with the naked eye. Such small voxels have about 4,000 times less signal than clinical systems. Imaging with MR in this microscopic domain has been achieved partly by the design of more efficient radiofrequency imaging coils, using stronger magnetic gradients (850 vs. 50 mT/m), and a higher magnetic field (7–14 vs. 1.5 T) (11). An additional problem with MRI of the lung is the effects of extensive air–tissue fluid interfaces, which result in severe susceptibility variation and cause a more rapid signal decay than occurs in solid tissues (10). The use of projection-encoding sequences can reduce the effective echo time to several hundred microseconds needed to capture the rapidly fading signals associated with the lung (12). Contrast agents (gadolinium [Gd] chelates) that shorten proton relaxation also improve the signal-to-noise ratio and shorten imaging times. The physics and engineering technology of MR may set the lower limits for spatial resolution in the range of 4 to 5 μm (13, 14). However, achieving these limits for the live animal depends on our attention to biological details. For animal imaging, biological motion from lungs, heart, and blood flow impose the final barriers to achieving the highest spatial resolution.

Mouse Lung—*Ex Vivo*

Microscopy, in its traditional form, examines specimens that are fixed, dehydrated, sliced, and chemically stained. MRM has several major advantages over these methods: (*1*) it is nondestructive, (*2*) it is three-dimensional, (*3*) it is inherently digital, and (*4*) the specimen remains hydrated (4).

In place of the chemical stains of light microscopy, MRM uses "stains" or enhancements of tissue structure contrast of a different sort (15). These stains consist of contrast agents that alter MR properties of the tissue to enhance structural contrast and imaging sequences that alter contrast based on MR properties of the tissue. Thus, with MRM, we do not have to physically cut, chemically stain, or dehydrate the specimen; the specimen can be imaged many times, in many planes, and can be viewed as a whole volume as originally preserved.

Figure 1 (p. 501) is an example from a fixed mouse specimen prepared by methods routinely used in our laboratory for imaging whole mice for morphologic phenotyping (15). These images are a set of thoracic transaxial slices extracted from a series of slices encompassing the entire body of a C57BL/6 female mouse (19 g). The animal was prepared by perfusing saline first and then 10% formalin through the body using catheters in the jugular vein and carotid artery. Both perfusion solutions contained MR contrast agent (Gd chelate, ProHance; Bracco Diagnostics, Princeton, NJ) (15). Peripheral vessels are used

for perfusion to minimize anatomic distortions of major organ systems and body cavities and particularly to avoid opening the chest. Thus, in this example, the lungs are fixed and stained while filled with air. Perfusion with the Gd chelate greatly shortens the MR T1 relaxation time, improves the signal-to-noise ratio, and shortens imaging time. A 7-T, 21-cm bore, Magnex magnet (EXCITE Console, version 11X; GE Medical Systems, Milwaukee, WI) was used for imaging, which required about 3 h for the entire mouse body. A 3D spin-echo sequence was used, which was modified from one previously described (15) to accommodate very large arrays. The matrix size was $512^2 \times 2{,}048$ pixels with voxel size of 63^3 μm^3 (0.25×10^{-3} mm^3).

Figure 1 (p. 501) shows detail of the lungs, at the sublobar level, of a normal mouse along with all the major cardiopulmonary vessels. The resolution is sufficient to identify pulmonary vessels and airways down to the fifth to sixth generation, the cardiac valves, coronary vessels, and a coronary artery. Because the image voxels are isotropic, we are able to follow structures level by level in all three major planes (axial, coronal, and sagittal) using computer software (ImageJ, V1.34S; National Institutes of Health, http://www.rsb.info.nih.gov/ij/). This is a valuable aid in tracing individual blood vessels and airways to verify structural continuity. Future studies using these methods will compare fine anatomic differences between mouse strains to identify morphologic phenotypic differences (normal and transgenic) and to evaluate the cardiopulmonary system challenged by toxicologic and teratologic agents.

Mouse and Rat Lung—*In Vivo*

All the problems associated with imaging fixed specimens, plus a few more, are present for the living animal. Motion from the heart and lungs is the biggest imaging challenge. Biological motion can easily degrade the image quality by blurring and by producing MR-related artifacts, such as ghosting (16). Some motion problems can be addressed by using extremely fast MRI sequences, such as radial spiral projection acquisitions (17) or by synchronizing the image acquisition to the phases of these biological motions (18). Assuming that the motion has a regular chronoperiodicity, by synchronizing to this motion we can essentially "see" the organ at the same phase of the cycle at each data sampling point. Simply gating imaging to the endogenous ECG cycle can be effective for cardiac imaging, but a similar approach for pulmonary imaging is less effective because of lung volume and breathing frequency changes during spontaneous breathing. Furthermore, because the lungs are constantly moved by the beating of the heart, highest-quality pulmonary imaging requires cardiac gating. This is particularly true at the spatial resolutions needed for small-animal imaging. The problem becomes challenging when we factor in the rates at which these events occur. In rats, heart rates can range from 300 to 500 beats/min, and breathing rates range from 50 to 70/min; in mice, heart rates range from 500 to 600 beats/min, and breathing rates range from 90 to 120/min.

Thus, highest-resolution lung imaging of these small animals requires exact and consistent control of the pattern of breathing and lung volumes, which can be achieved only with mechanical ventilation and cardiac gating. For the traditional pulmonary physiologist, having mechanical ventilation for small animals is not a problem, but for one working with small animals in high magnetic fields (≥ 2 T), it is a big problem. Because of the many exciting possibilities for lung research, we have devoted much effort to building MR-compatible small-animal ventilators (18–20). Using MR-compatible ventilation to support lung imaging, the lung volume and frequency of breathing can be controlled consistently over the period of the MRI acquisition, which may last for a few to many minutes.

Figure 2 (p. 502) shows schematically how MRI acquisitions can be synchronized to the cardiac and breathing cycles for highest-resolution images of heart and lungs. This synchronization is achieved using custom-written LabVIEW (National Instruments, Austin, TX) applications running on a computer that controls the ventilator breathing cycle (Figure 2A) and generates an enabling window (user-specified) to allow ECG triggering at a specified phase of the breath cycle (end expiration or peak inspiration). When a QRS spike (Figure 2B) occurs during that window, a trigger (Figure 2D) is generated to initiate the MR scan sequence (Figure 2E). In addition, the cardiac trigger can be placed at any point during the R-to-R interval to obtain images at selected times of the cardiac cycle (Figure 3). Figure 3 is a projection acquisition of rat thorax using combined ventilation and cardiac synchronization (7).

Although the quality of images produced by this method of synchronizing imaging to biological motion is a testimony to its effectiveness, we have quantitatively assessed the precision of this method. We measured how consistently the diaphragm of the rat returned to the same point at each breath (21). The excursion of metal beads cemented to the abdominal surface of the diaphragm with reference to a stationary bead on spinal column was measured using an X-ray system with in-plane resolution of 20 μm. The animals were ventilated on the X-ray system exactly as they would be in MR using the same type of ventilator and breathing control. We found the maximum excursion of the dome of the diaphragm from full-inspiration to end-expiration was about 2 mm. We concluded that our motion control was effective to within the 100-μm resolution limits of our MRI.

A disadvantage of conventional, noninvasive imaging methods, such as X-ray or MRI, is that these methods do not directly image the airspaces of the lung because of low X-ray attenuation or absence of proton signal. However, the lung consists mostly of gas spaces, up to 80% of total lung volume. With the advent of polarized, noble gas imaging with MR (22), we have the advantage of being able to image the entire lung, including gas and tissue. With our mechanical ventilation system, we can remotely change the mixture of breathing gases and deliver carefully controlled volumes of hyperpolarized ^{3}He to the animal in synchrony with the imaging sequence. With the animal in a stable position in a dual-frequency coil (Figure 4 [p. 502]), we can perform proton ^{1}H and ^{3}He imaging in a single session at high resolution.

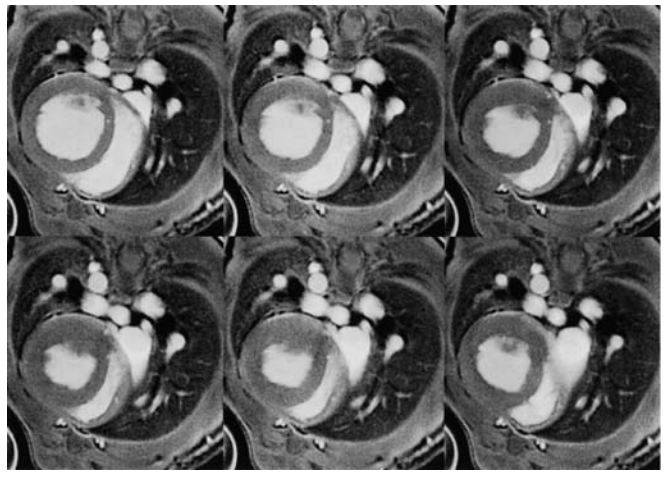

Figure 3. Projection-acquisition images from an anesthetized rat at six points of the cardiac cycle progressing from the QRS spike to the end of the R-to-R interval in 20-ms steps. Reprinted with permission from Reference 7.

Figure 5 (p. 502) shows the application of this strategy of using two signal sources to image the lung of a live, anesthetized rat. A coronal section of the thorax of a live anesthetized rat shows ^{3}He in the gas spaces of the lung and extrapulmonary airways (Figure 5, *right*) in exact registry with a proton image (^{1}H; Figure 5, *center*). The image on the right shows how both of these images can be superimposed to aid in identifying exact anatomic relationships between these important components of the lungs. For these images, we use a dual-frequency radiofrequency coil tuned for proton (^{1}H) and ^{3}He resonances. This coil eliminates the need to change the animal's position during the imaging and allows us to change the animal's breathing of normal air to a mixture of air and hyperpolarized ^{3}He without disturbing the animal. ^{3}He was polarized using an optical method and imaged by methods described in more detail by Johnson and colleagues (23).

The power of dual-compartment, MRI (tissue ^{1}H and gas ^{3}He) of the lung is illustrated in a study on the effect of therapeutic radiation on the lung (24). By performing proton and ^{3}He imaging on the animal's lung in the same session, we are able to maintain anatomic registration for analysis of regional morphology of the injury pattern. The tissue and airway compartments are shown in Figure 6 (p. 502) (24). The proton image (Figure 6A) suggests damage to the right lung, which is even more clearly apparent in the ^{3}He image (Figure 6B). An additional advantage of these imaging methods is being able to quantitate the changes in microstructure of the lung by measuring the apparent diffusion coefficient (ADC) of ^{3}He in lungs. During the weeks after irradiation, there was a progressive decrease in ADC, reflecting a greater restriction of the He diffusion space associated with the progressive development of fibrosis that was confirmed by conventional histology (Figures 6C and 6D).

Another example of small-animal lung imaging examined elastase injury as a model for emphysema (25). Only minimal changes were detected in proton images, whereas increasing values of ^{3}He ADC clearly indicated a change in the lung's microstructure associated with less restriction of He diffusion, reflecting the increased alveolar size and increased stiffness of the lung—classical signs of emphysema.

CONCLUSIONS

MRM has become a valuable tool to study the small-animal lung. Its strength lies in its ability to visualize noninvasively and at high resolution the morphology of the normal and injured lung. A further strength of MRM is that it lends itself to longitudinal studies because of noninvasive instrumentation, life support during imaging, and use of anesthetics that allow rapid recovery. The future will bring further improvements in technology that will allow us, one day, to image individual alveoli in these small animals.

Conflict of Interest Statement: Neither of the authors has a financial relationship with a commercial entity that has an interest in the subject of this manuscript.

Acknowledgment: The authors thank their colleagues in the Duke Center for In Vivo Microscopy for their many contributions to the work described. The authors also thank Ms. Boma Fubara, Mr. Gary Cofer, Ms. Sally Gewalt, Mr. William Kurylo, and Ms. Sally Zimney for manuscript preparation.

References

1. Bock NA, Zadeh G, Davidson LM, Qian B, Sled JG, Guha A, Henkelman RM. High-resolution longitudinal screening with magnetic resonance imaging in a murine brain cancer model. *Neoplasia* 2003;5:546–554.
2. Itter G, Jung W, Juretschke P, Schoelkens BA, Linz W. A model of chronic heart failure in spontaneous hypertensive rats (SHR). *Lab Anim* 2004;38:138–148.
3. Beckmann N, Mueggler T, Allegrini PR, Laurent D, Rudin M. From anatomy to the target: contributions of magnetic resonance imaging to preclinical pharmaceutical research. *Anat Rec* 2001;265:85–100.
4. Maronpot RR, Sills RC, Johnson GA. Applications of magnetic resonance microscopy. *Toxicol Pathol* 2004;32:42–48.
5. Johnson GA, Cofer GP, Fubara B, Gewalt SL, Hedlund LW, Maronpot RR. Magnetic resonance histology for morphologic phenotyping. *J Magn Reson Imaging* 2002;16:423–429.
6. Dazai J, Bock NA, Nieman BJ, Davidson LM, Henkelman RM, Chen XJ. Multiple mouse biological loading and monitoring system for MRI. *Magn Reson Med* 2004;52:709–715.
7. Hedlund LW, Gewalt SL, Cofer GP, Johnson GA. MR microscopy of the lung. In: Cutillo A, editor. Application of magnetic resonance to the study of the lung. Mt. Kisco, NY: Futura Publishing; 1996. pp. 401–415.
8. Tigani B, Schaeublin E, Sugar R, Jackson AD, Fozard JR, Beckmann N. Pulmonary inflammation monitored noninvasively by MRI in freely breathing rats. *Biochem Biophys Res Commun* 2002;292:216–221.
9. Chen BT, Johnson GA. Dynamic lung morphology of methacholine-induced heterogeneous bronchoconstriction. *Magn Reson Med* 2004; 52:1080–1086.
10. Cutillo AG. Application of magnetic resonance to the study of lung. Armonk, NY: Futura Publishing; 1996.
11. Johnson GA, Benveniste H, Black RD, Hedlund LW, Maronpot RR, Smith BR. Histology by magnetic resonance microscopy. *Magn Reson Q* 1993; 9:1–30.
12. Gewalt SL, Glover GH, Hedlund LW, Cofer GP, MacFall JR, Johnson GA. MR microscopy of the rat lung using projection reconstruction. *Magn Reson Med* 1993;29:99–106.
13. Cho ZH, Ahn CB, Juh SC, Lee HK, Jacobs RE, Lee S, Yi JH, Jo JM. Nuclear magnetic resonance microscopy with 4-micron resolution: theoretical study and experimental results. *Med Phys* 1988;15:816–824.
14. Cofer GP, Brown JM, Johnson GA. *In vivo* magnetic resonance microscopy at 5 microns. *J Magn Reson* 1989;83:608–616.
15. Johnson GA, Cofer GP, Gewalt SL, Hedlund LW. Morphologic phenotyping with magnetic resonance microscopy: the visible mouse. *Radiology* 2002;222:789–793.
16. Wood M, Henkelman R. NMR image artifacts from periodic motion. *Med Phys* 1985;12:143–151.
17. Brau ACS, Hedlund LW, Johnson GA. Cine magnetic resonance microscopy of the rat heart using cardiorespiratory-synchronous projection reconstruction imaging. *J Magn Reson Imaging* 2004;20:31–38.
18. Hedlund LW, Cofer GP, Owen SJ, Allan Johnson G. MR-compatible ventilator for small animals: computer-controlled ventilation for proton and noble gas imaging. *Magn Reson Imaging* 2000;18:753–759.
19. Hedlund LW, Deitz J, Nassar R, Herfkens R, Vock P, Dahlke J, Kubek R, Effmann E, Putman C. A ventilator for magnetic resonance imaging. *Invest Radiol* 1986;21:18–23.
20. Chen BT, Brau ACS, Johnson GA. Measurement of regional lung function in rats using hyperpolarized 3Helium dynamic MRI. *Magn Reson Med* 2003;49:78–88.
21. Mai W, Badea CT, Wheeler CT, Hedlund LW, Johnson GA. Effects of breathing and cardiac motion on the spatial resolution in microscopic imaging of rodents. *Magn Reson Med* 2005;53:858–865.
22. Moller HE, Chen XJ, Saam B, Hagspiel KD, Johnson GA, Altes TA, de Lange EE, Kauczor HU. MRI of the lungs using hyperpolarized noble gases. *Magn Reson Med* 2002;47:1029–1051.
23. Johnson GA, Cofer GP, Hedlund LW, Maronpot RR, Suddarth SA. Registered ^{1}H and ^{3}He magnetic resonance microscopy images of the lung. *Magn Reson Med* 2001;45:365–370.
24. Ward ER, Hedlund LW, Kurylo WC, Wheeler CT, Cofer GP, Dewhirst MW, Marks LB, Vujaskovic Z. Proton and hyperpolarized helium magnetic resonance imaging of radiation-induced lung injury in rats. *Int J Radiat Oncol Biol Phys* 2004;58:1562–1569.
25. Chen XJ, Hedlund LW, Moller HE, Chawla MS, Maronpot RR, Johnson GA. Detection of emphysema in rat lungs by using magnetic resonance measurements of 3He diffusion. *Proc Natl Acad Sci USA* 2000;97: 11478–11481.

MORPHOLOGY OF THE SMALL-ANIMAL LUNG USING MAGNETIC RESONANCE MICROSCOPY
Laurence W. Hedlund and G. Allan Johnson (pages 481–483)

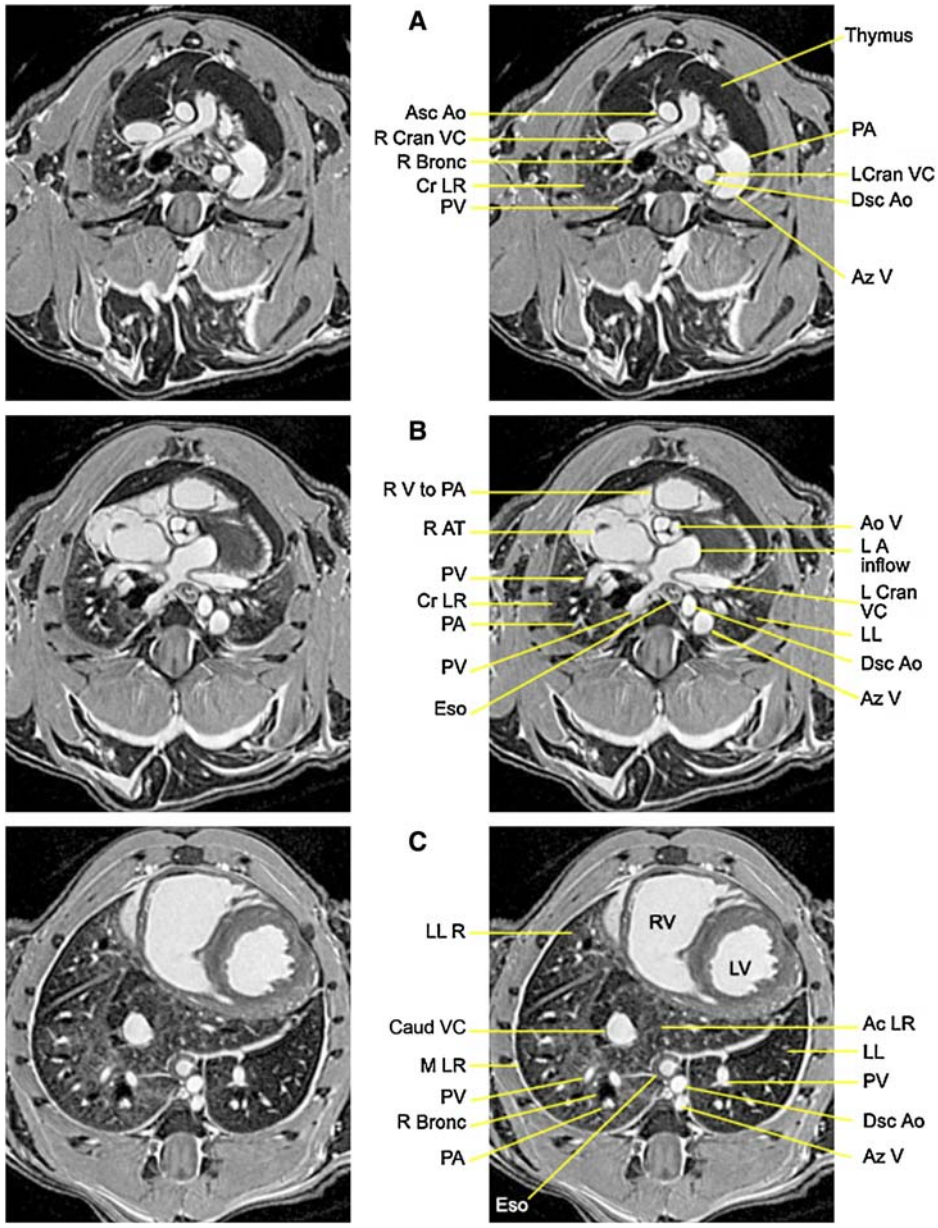

Figure 1. (*A*–C) Axial views of a 19-g mouse showing major thoracic structures from most cranial level (*A*) to the most caudal level (*C*). Images on the *right* show labels for the same images on the *left*. Right lung: AC LR = accessory lobe; Ao V = aortic valve; Asc Ao = ascending aorta; AZ V = azygous vein; Caud VC = caudal vena cava; Cr LR = cranial lobe right; Dsc Ao = descending aorta; Eso = esophagus; L Cran VC = left cranial vena cava; LA = left atrium; LL = left lung; LLR = lower/caudal lobe; LV = left ventricle; MLR = middle lobe; PA = pulmonary artery; PV = pulmonary vein; R Cran VC = right cranial vena cava; RA = right atrium; RV = right ventricle. Separation in mm between levels: *A*–*B* = 1.13; *B*–*C* = 3.4; total (*A*–C) = 4.6 mm, slice thickness = 0.063 mm.

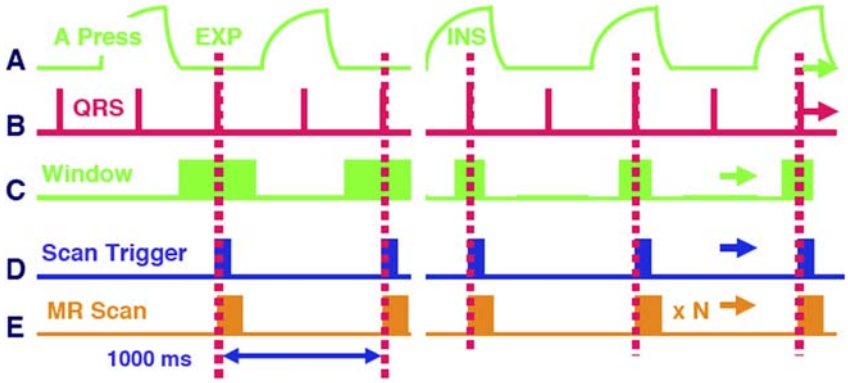

Figure 2. (*A–E*) Schematic waveforms illustrate how magnetic resonance imaging (MRI) data acquisition (*E*) is triggered (*D*) in synchrony with the cardiac cycle (*B*) and breathing cycle (*A*) during expiration (EXP) or inspiration (INS). *Left side* shows imaging during EXP. *Right side* shows imaging during peak INS.

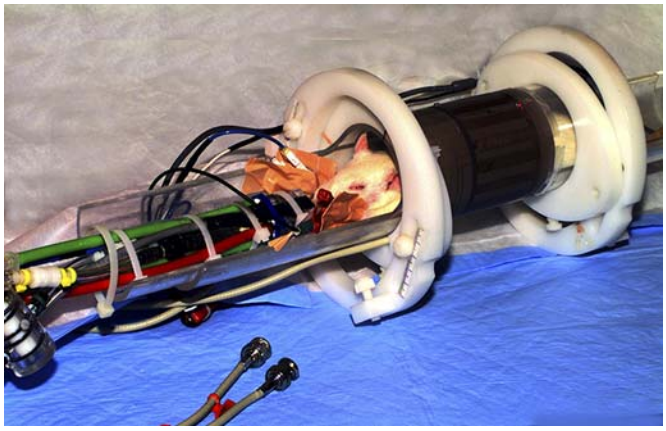

Figure 4. Anesthetized 250-g rat positioned in a Plexiglas cradle (6.3-cm diameter) supported by white Delrin rings (15-cm diameter) for imaging in a 2-T magnet with a 15-cm diameter bore. The transmit/receive radiofrequency imaging coil is seen covering the chest and abdomen positioned between the white support rings. The coil operates at two frequencies for hydrogen and helium imaging. The animal's endotracheal tube is connected directly to an MR-compatible breathing valve, which is connected to power and breathing air supply hoses. The animal is instrumented with ECG electrodes attached to the paws and rectal temperature probe.

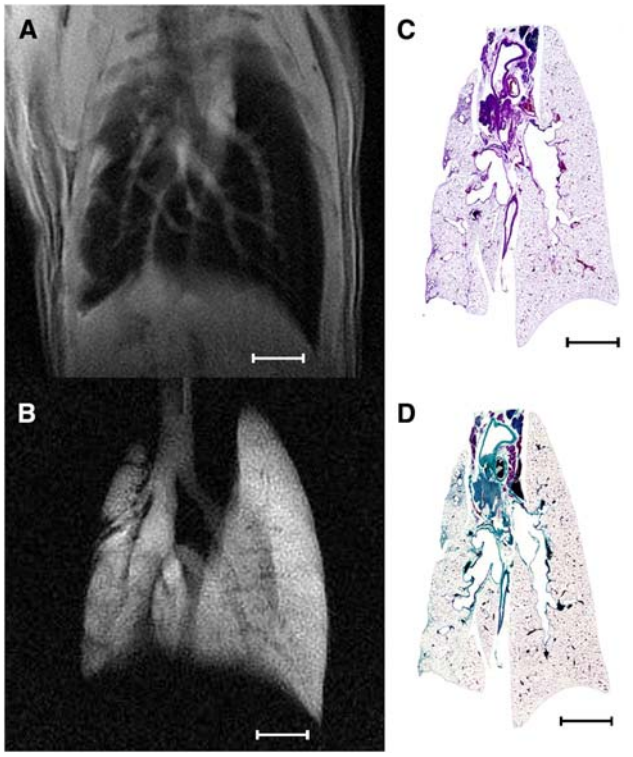

Figure 6. Coronal images of a rat 6 mo after right lung irradiation. (*a*) ^{1}H, (*b*) ^{3}He, (*c*) hematoxylin and eosin (H&E), and (*d*) Masson's trichrome show significant damage to the right lung. Damage seen in the *in vivo* MRI corresponds to areas of severe fibrosis found on H&E and Masson's sections. *Bar*, 5 mm. Reprinted with permission from Reference 24.

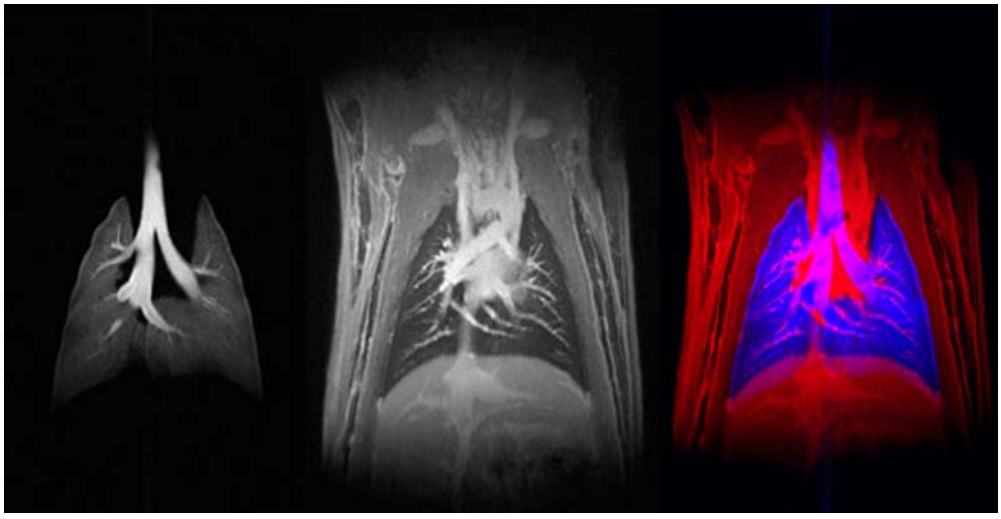

Figure 5. Coronal slabs (five 2-mm slices combined, 100 μm in-plane) from an anesthetized live rat being respirated with a combination of hyperpolarized ^{3}He and air (*left*) or air only (*center*). Both images are shown superimposed on the *right*. For details, *see* Johnson and colleagues (23).